

Assessment of 21 years of Arctic Ocean Absolute Sea Level Trends (1995-2015)

Carsten Ankjær Ludwigsen¹, Ole Baltazar Andersen¹, and Stine Kildegaard Rose¹

¹DTU Space, Elektrovej 328, 2800 Kgs. Lyngby, Denmark

Correspondence: Carsten Ankjær Ludwigsen (caanlu@space.dtu.dk)

Abstract. The Arctic Ocean is at the frontier of the fast changing climate in the northern latitudes. As the first study, we assess the different mass and steric components of the observed sea level trend from both absolute sea level (ASL) from altimetry and tide gauges (TG), without using gravimetric observations from the GRACE satellites Gravity Recovery and Climate Experiment (GRACE). This approach permits a longer time series and avoids problems with errors from leakage effects in GRACE-products. The ASL is equal to the mass-driven sea level and the steric sea level, while tide gauge based sea level is also affected by associated with GRACE. Steric and manometric sea level change is reconstructed and is combined into an Arctic sea level estimate, that is independent from any observed sea level change. Relative sea level observed by 12 selected tide gauges is corrected with novel vertical land movement, which is in this study correct by novel estimates. Calculations of the mass component from present-day deglaciation, shows that deglaciation rises Arctic sea level with more than 1 (VLM) estimates accounting for past and contemporary deglaciation. The calculations shows that contemporary deglaciation alters the Arctic absolute sea level between 0 and 2 mm y⁻¹, while the steric contribution is between -5 and 15 salinity-driven halosteric sea level trend is dominating the sea level trend with variations between -7 and 10 mm y⁻¹ with large spatial variability and dominated by the halosteric signal. A dynamic mass contribution is derived from the Estimating Circulation and Climate of the Oceans (ECCO)-model (version 4, release 4), which varies between -1 and 2 mm y⁻¹. The combined mass and steric product.

Large uncertainties originate from limited data to constrain the steric data in some regions of the Arctic while also altimetry is visibly challenged in sea ice covered areas. The reconstructed sea level estimate agrees (within uncertainty) with ASL-trends observed the observed sea level from altimetry in 9998% of the Arctic, although large uncertainties originate from poor data coverage in the steric data and large variability in the dynamic product. A comparison with ASL-trends observed at tide gauges agree with mass+steric at and for 11 of 12 tide gauge sites-TGs. The correlation between the reconstructed estimate and altimetry (R=0.50) clearly outperforms a similar study using GRACE-estimates. The results confirm a large negative absolute sea level trend shown by other studies in the eastern Siberian Arctic, that is in contrast to the significant sea level rise observed in the area by TGs

1 Introduction

- 25 The Arctic is globally the region with the fastest changing climate and is warming twice the rate of the global average (Box et al., 2019). The resulting ~~enhanced~~ deglaciation of land ~~and sea ice~~, ~~sea ice cover decrease~~ and ocean freshening ~~all changes the has several affects on~~ sea level, hence understanding sea level in the Arctic Ocean paramount for mapping consequences of climate change. ~~At the same time, oceanographic in-situ observations and satellite observations of the Arctic are prone to challenges from an harsh environment, sea ice floats and lack of spatial coverage (Smith et al., 2019).~~
- 30 ~~Spatial assessments of the sea level budget of the Arctic has in previous studies~~ Satellite altimetry has been measuring the Arctic Ocean since 1991 with ESA's European Remote Sensing (ERS)-1 satellite being the first reaching polar latitudes. (Laxon et al., 2003) were the first to study Arctic sea level from the ERS-1/2 satellites to produce sea-ice thicknesses. Since then many have followed e.g. (Peacock and Laxon, 2004; Prandi et al., 2012; Cheng et al., 2015; Rose et al., 2019), but uncertainties in particular in sea ice-covered regions are still present (Armitage et al., 2016; Rose et al., 2019; Raj et al., 2020).
- 35 ~~Reconstructing sea level change with the sea level budget is useful both to constrain sea level observations and separate steric-driven and manometric sea level change (Gregory et al., 2019) and hence quantify the origins of sea level change. The sea level budget has been assessed on global and basin-wide scales since the 19th century by using a combination of in-situ data, satellite observations and probabilistic analysis (Church and White, 2011a; WCRP, 2018; Dangendorf et al., 2019; Royston et al., 2020; Fr~~, but these studies tends to neglect the polar region.
- 40 ~~Previous attempts to reconstruct sea level in the Arctic has~~ shown to be difficult (Henry et al., 2012; Armitage et al., 2016; Carret et al., 2017; Ludwigsen and Andersen, 2020; Raj et al., 2020), because both satellite observations and in-situ observations are less consistent than in low and mid-latitudes ~~and challenged by the Arctic environment and fast-changing climate~~. Observations from the Gravity Recovery And Climate Experiment (GRACE) offer the only direct Arctic-wide measurements of ~~the mass component, but manometric sea level change since mid-2002~~. However, discrepancies of over 10 mm y^{-1} (Ludwigsen and Andersen, 2020) exist among different GRACE-products (Wiese et al., 2016; Save et al., 2016; Lutheke et al., 2013), and previous studies often ~~tend to~~ choose the solution that ~~fits the altimetric results (Carret et al., 2017; Raj et al., 2020)~~ ~~-A cross-comparison of different combinations of GRACE, steric products and altimetry (Ludwigsen and Andersen, 2020)~~ ~~-showed that the~~ has the best agreement with the absolute sea level observed by altimetry and modeled steric sea level (Carret et al., 2017; Raj et al., 2020).
- 50 ~~In this paper, we attempt to assess the satellite and tide gauge observed Arctic sea level budget using an interpolated DTU steric product and a mass-product from the GRACE satellites (GRACE JPL mascons (Wiese et al., 2016)) for 2003 to 2015 agreed well spatially with an altimetry-product from CPOM (Armitage et al., 2016)-trends from 1995-2015 by reconstructing the sea level response to contemporary land ice loss, glacial isostatic adjustment (GIA) and atmospheric pressure (inverse barometer, IB) and thereby mapping the long-term manometric sea level change without GRACE. The time series of 21~~
- 55 ~~years is generally 8 years more than assessments using GRACE (Armitage et al., 2016; Carret et al., 2017; Raj et al., 2020). This has the advantage, that non-secular and inter-annual dynamic effects, which are mainly driven by the Arctic Oscillation, (Henry et al., 2012; Armitage et al., 2018) are reduced.~~

2 Method

60 Sea level observations from satellite altimetry are measured relative to a terrestrial reference frame and is called geocentric or absolute sea level (ASL) can be divided into two main contributions; changed water column density. Tide gauges (TG) measures the sea level while being grounded to the coast, and is affected by vertical land movement (VLM). The ASL (similar to altimetry) can be reconstructed by adding vertical land movement (VLM), defined with respect to the same reference frame as altimetry, to tide gauge-measured relative sea level (RSL).

$$65 \quad \underline{ASL = RSL + VLM} \quad (1)$$

Changes of ASL (\dot{ASL}) originates either from changed ocean density (steric, $\dot{\eta}$) due to changes in salinity or temperature (halosteric) or temperature (thermosteric) or from changes in ocean mass, which is called steric change and mass change (also called defined as manometric sea-level change, \dot{M} (Gregory et al., 2019)). According to (Gregory et al., 2019), manometric sea level change can be referred to as the 'non-steric' sea level change and is indifferent to the commonly used Ocean Bottom Pressure) due to changes of (OBP).

$$\underline{\dot{ASL} = \dot{\eta} + \dot{M}} \quad (2)$$

As already mentioned, the steric sea level change can be split into halosteric ($\dot{\eta}_S$) and thermosteric ($\dot{\eta}_T$) sea level change:

$$\underline{\dot{\eta} = \dot{\eta}_S + \dot{\eta}_T} \quad (3)$$

65 The manometric component is further divided into contributions from changes in the gravitational field, G that together with a spatial uniform constant, c , composes the gravitational sea level fingerprint (N) due to different land-to-ocean water mass flux and dynamic changes from changing wind stress and atmospheric pressure.

$$\underline{\dot{ASL} = \text{Steric} + \text{Mass}}$$

80 mass changes, i , which in this study originates from either different sources of land ice (Greenland (GRE), Northern Hemisphere (NH) Glaciers and Antarctica (Ant) + Southern Hemisphere (SH) glaciers) or GIA. Change in IB is also part of the total manometric sea level change, \dot{M} .

$$\underline{\dot{M} = \sum_i \dot{N}_i + \dot{IB}} \quad , \quad \text{where} \quad \underline{\dot{N}_i = \dot{G}_i + \dot{c}_i} \quad (4)$$

Tide gauges (TG) gives direct measurements of sea level relative to the solid earth -- called relative sea level (RSL). ASL measured by satellite altimetry is measured relative to the Earth's center. The difference between ASL and RSL is defined

85 ~~by the deformation of the solid Earth—called vertical land movement (VLM). VLM is split into the viscoelastic solid earth deformation caused from past millennial ice (un-)loading, GIA, and the elastic adjustment from contemporary (1995-2015) change in ice loading, VLMe, which, as \dot{G} , is a composite of the elastic response from different origins of land ice (i).~~

$$\underline{ASL_{VLM}} = \underline{RSL_{GIA}} + \underline{VLM} \sum \underline{VLMe}_i \quad (5)$$

90 ~~GRACE was first launched in mid 2002. Bypassing GRACE makes it possible to extend the time series to 21 years from 1995-2015, which generally is 8 years more than assessments using GRACE (Armitage et al., 2016; Carret et al., 2017; Raj et al., 2020). This has the advantage, that non-secular and non-seasonal effects of the Arctic Oscillation, which tends to dominate the dynamic mass contribution (Henry et al., 2012; Armitage et al., 2018) gets smaller. By substituting eq. 4 and eq. 3 into eq. 2, we achieve the reconstruction of absolute sea level, ASL_r , that is comparable with the observed ASL by satellite altimetry (denoted as ASL_A):~~

$$\underline{ASL_r} = \sum (\underline{\dot{G}_i} + \underline{\dot{c}_i}) + \underline{\dot{B}} + \underline{\dot{\eta}_S} + \underline{\dot{\eta}_T} \quad (6)$$

95 3 Altimetry

~~Thirdly, a TG-based ASL estimate, ASL_{TG} , is achieved by adding eq. 5 to eq. 1:~~

$$\underline{ASL_{TG}} = \underline{RSL_{TG}} + \underline{GIA} + \sum \underline{VLMe}_i \quad (7)$$

3 Data

100 ~~This study combines various in-situ data (temperature and salinity (T/S) profiles and TG-data), satellite (GRACE and altimetry) and model data (VLM-model and ECCOv4r4) to reconstruct the Arctic sea level change. In this section follows a description of the different datasets and how they are obtained.~~

3.1 Altimetry

105 ~~The DTU/TUM Arctic altimetric dataset Ocean Sea Level Anomaly (SLA) record (Rose et al., 2019) provides an independent estimate of ASL change. For the 1995-2015 period, both (ASL_A). The altimetric time series is covering the whole altimetric era given as monthly grids from September 1991 to September 2018, covering 65° N to 81.5°N and 180°W–179.5°E.~~

~~The product is corrected by geophysical corrections such as tides and atmospheric delays. Leads (cracks in the sea ice cover) and open ocean are located and separated according to the different classification of their surfaces. The detection of leads is not flawless, and their sparse distribution in the sea ice cover, and the uncertainty of the the applied geophysical corrections in the Arctic (Stammer et al., 2014; Ricker et al., 2016) makes the sea level estimates more uncertain in the sea ice covered region.~~

110 The altimetric record includes data from four ESA satellites: ERS-1 (1991-1995), ERS-2 (1995-2003), Envisat (limited to 81.5°N 2002-2010) and CryoSat-2 (limited to 88°N) is used 2010-2018. It combines results of different retracers as well as conventional and SAR-altimetry, which may lead to biases (Rose et al., 2019). In particular ERS-1/2 has a relative relatively low spatial resolution and thereby limiting the measurements from leads (~~open-ocean-in-between-the-sea-ice-floes~~) in sea ice. ~~Also difficulties to distinguish between melt ponds on top of,~~ while the SAR altimeter on CryoSat-2 is made to measure over the sea ice ~~and leads were shown to be difficult. The used DTU cover, which decreases the uncertainty (Rose et al., 2019). The applied version of the DTU/TUM altimetry product is not corrected for IB and is spatially limited southward to 65°N atmosphere pressure loading to be able to compare to the tide gauges.~~ The altimetric sea level trend is shown in the ~~right map results section (the middle panel of figure 5).~~

4 **Tide Gauge data**

120 ~~Tide gauges-~~

3.1 Tide Gauges and Vertical Land Movement

TG-data is obtained from the Permanent Service of Sea Level (PSMSL)-database (Holgate et al., 2012) given as monthly SLA. TGs with a consistent time series are few and unevenly distributed in the Arctic (Henry et al., 2012; Limkilde Svendsen et al., 2016). Locations with both TG and GNSS to measure VLM is even rarer. As a substitute for GNSS-measurements, we correct
125 ~~TG with the~~ Usually, TG-observed RSL is aligned to ASL by utilizing vertical velocities from a nearby Global Navigation Satellite System (GNSS) receiver. Restricting TGs to locations with usable GNSS significantly limits the selection further. Therefore, an Arctic-wide VLM-model described in (Ludwigsen et al., 2020a), which offers accurate VLM predictions for the Arctic area (Ludwigsen et al., 2020a) as a substitute for GNSS is applied (figure 1).

Twelve TG's are selected in the Arctic region from the PSMSL-database (Holgate et al., 2012) (displayed in The VLM-model
130 is composed from eq. 5. The GIA-component is based on the Caron2018 GIA-model (Caron et al., 2018), which includes an uncertainty estimate. Reported discrepancies from other GIA-models in central North America and Greenland (Caron et al., 2018; Ludwigsen et al., 2020a) has little affect at the locations of TGs of this study. Annual rates of VLMe is estimated from the 1995-2015 annual change of land ice using the Regional Elastic Rebound Calculator (REAR) (Melini et al., 2015). REAR also provides the gravitational response G to land ice change used for estimating the manometric sea level. Uncertainties of the elastic VLM-estimates are
135 mainly due to uncertainties of the applied land ice change. An additional 10% of the VLM-signal (after Wang et al. (2012)) is added to represent uncertainties associated with the REF6371 Earth model (Kustowski et al., 2007) applied in REAR. The VLM contribution from non-tidal ocean loading (NOL) (van Dam et al., 2012) and rotational feedback (RF) (King et al., 2012) are in total of an order of $\pm 0.3 \text{ mm y}^{-1}$ and are included in the VLM-contribution from Northern Hemisphere glaciers.

12 TGs are selected (geographical locations shown in figure 1) .The selection is based on visual inspection of the monthly
140 time series and to ensure that as many regions of the Arctic is represented as possible. A 3-month averaged time series from and linear trend of TG observed sea level (RSL_{TG}) and VLM-corrected sea level (ASL_{TG}) from 1995-2015 of every TG and

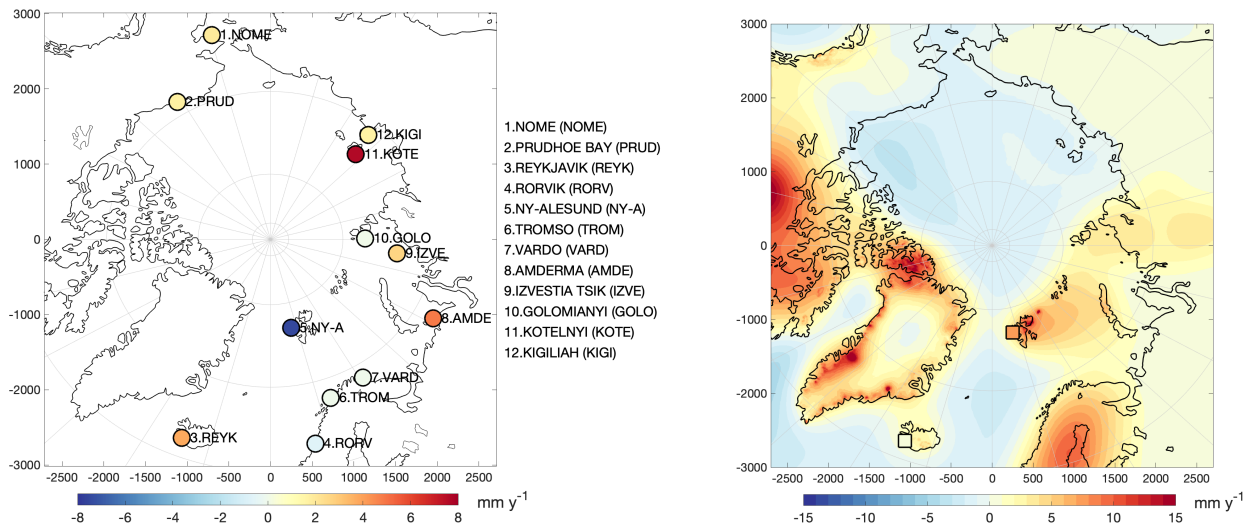


Figure 1. Left: 1995-2015 RSL trend [mm y^{-1}] and location of the selected tide gauges of this study. Right: 1995-2015 VLM-trend [mm y^{-1}] from the model of Ludwigsen et al. (2020b). The VLM-trend from the GNSS-sites at Reykjavik and Ny-Ålesund is-are shown with squared color coded markers.

the linear trend is shown in figure 2. The annual VLM-model is interpolated onto the TG time series and the linear trend is determined with least-squares method using months with available data between 1995 and is-corrected for VLM by using the 2015. In particular, the Alaskan and Siberian TGs have months with no or unreliable data (flagged by PSMSL). However, there
 145 is no evident seasonality in the missing months and therefore does not significantly affect the trend-estimates with a seasonal bias.

Ny-Ålesund and Reykjavik TG experience extraordinary VLM that is caused by substantial deglaciation during the Little Ice Age (LIA) (Svalbard) and low mantle viscosities in Iceland and Greenland. This is not captured in the spatially uniform REF6371 earth model. Therefore, the two sites are corrected with nearby GNSS (Global Navigation Satellite System) instead of
 150 the VLM-model. GNSS is uncertain at Prudhoe Bay, where it measures a significant subsidence, that is considerably different from the VLM-model(Ludwigsen et al., 2020b) or-, as in the case for Ny-Alesund and Reykjavik, using nearby GNSS for VLM(see figure 1). This is likely caused by near-by construction or oil depletion sites. However, the tide gauge is located on a peninsula reaching into the Beaufort Sea 10 km away from the GNSS-location, which is why the VLM-model is trusted over the GNSS-measurement.

155 Reykjavik (64.2°N), Nome (64.5°N), and Rorvik (64.9°N) are located off the edge of the DTU/TUM Arctic altimetry dataset (Rose et al., 2019) altimetric data, which only extends to 65°N , but are nevertheless included to extend the spatial distribution of the TG-sites.

TG-trends are determined with least-squares method using months with data between 1995 and 2015 and the VLM-correction is interpolated onto the monthly TG-time series. From figure 2, we see that trends-the RSL-trends in the Arctic vary with

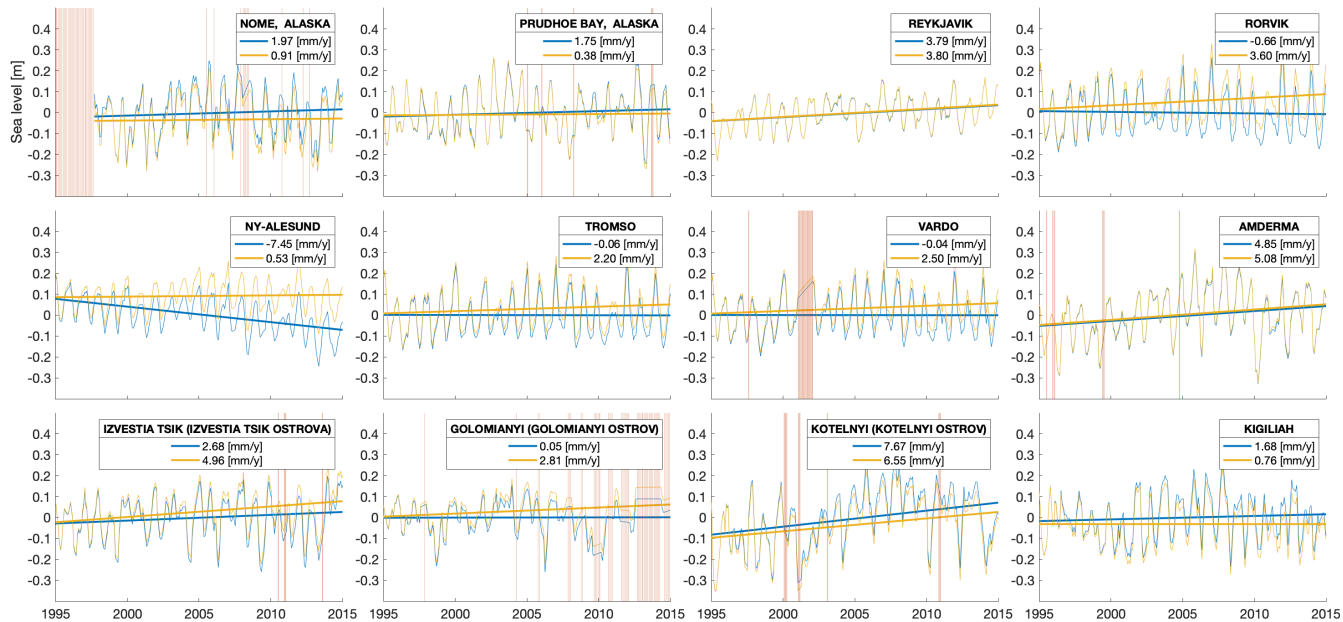


Figure 2. Relative sea level [m] from 1995-2015 registered at the 12 tide gauge from the PSMSL-database (Holgate et al., 2012)]. Blue line represents the 3-month running average, while the thick line is the linear trend (trend estimate [mm y^{-1}] shown in legend). Yellow line represents the absolute sea level and trend, equal to the blue line corrected for VLM with a VLM-model (Ludwigsen et al., 2020b) (except Ny-Ålesund and Reykjavik that are corrected with GNSS). The vertical lines indicate where observations are missing and the sea level is linearly interpolated from adjacent months.

160 nearly $\pm 1 \text{ cm y}^{-1}$, with Ny-Ålesund on Svalbard having a negative ~~sea-level-trend~~ RSL-trend of -7.45 mm y^{-1} , while Kostelny Island between the Laptev and East Siberian Sea shows a positive trend of 7.67 mm y^{-1} . However, after applying the VLM-correction, does all TGs show a positive ASL-trend within a range of 0.3 mm y^{-1} (Prudhoe Bay) and 6.5 mm y^{-1} (Kostelny).

3.2 Steric sea level

165 The DTU steric sea level change is computed as described in Ludwigsen and Andersen (2020). The steric sea level change is computed from a three dimensional T/S-grid that is interpolated from a over 300.000 T/S profiles and thus not constrained by any satellite observations. ~~The VLM-model utilizes the Caron2018 GIA-model (Caron et al., 2018) which is added to an annual elastic VLM-model from 1995-2015 change in present-day ice loading (PDIL). As shown in Ludwigsen and Andersen (2020), Ny-Ålesund and Reykjavik experience extraordinary VLM, caused by substantial deglaciation during the Little Ice Age (Svalbard) and low mantle viscosities (Iceland and Greenland), that is not restored in the VLM-model. Therefore, are the two sites corrected with nearby GNSS instead of the VLM-model. GNSS is uncertain at Prudhoe Bay, where it measures a significant subsidence, that is significantly different from the VLM-model. This is probably caused by near-by construction~~

170

or oil depletion sites. However, the tide gauge is located on a peninsula reaching into the Beaufort Sea 10 km away from the GNSS location, which is why the VLM-model is trusted over the GNSS-measurement.

175 4 Steric contribution

The DTU-independent steric sea level change is computed as described in Ludwigsen and Andersen (2020). Salinity and temperature measurements estimate is in contrast to Morison et al. (2012) and Armitage and Davidson (2014), that use a difference between altimetry and GRACE to estimate steric heights.

T/S-profiles from buoys, ice-tethered profiles and ship expeditions in the Arctic Ocean are spatial and temporal unevenly distributed and also depends on seasonal accessibility (Behrendt et al., 2017). Especially, the data density is poor in the shallow seas along the Siberian Coast (Ludwigsen and Andersen, 2020), which is cause to large uncertainties. Temperature and salinity data are interpolated by kriging into a monthly 50x50 km spatial grid on 41 depth levels. If values are more than 3σ away from the mean of neighbouring grid cells, values from the same month in adjacent years is used.

Following the notion of Gill and Niller (1973); Stammer (1997); Calafat et al. (2012); Ludwigsen and Andersen (2020), the change in steric heights, η , are sea level is calculated as the sum of halosteric heights (the contribution from salinity change) sea level, η_S and thermosteric heights sea level, η_T :-

$$\dot{\eta} = \dot{\eta}_S + \dot{\eta}_T$$

Depth profiles from (equation 3). From the depth profiles of the temperature and salinity grids are used for computing the right-hand side of equation 3 grid, η_S and η_T are calculated:

$$190 \quad \eta_S = -\frac{1}{\rho_0} \int_{-H}^0 \beta S' dz \quad (8)$$

$$\eta_T = \frac{1}{\rho_0} \int_{-H}^0 \alpha T' dz \quad (9)$$

where H denotes the minimum height (maximum depth (z)). S' and T' are defining salinity and temperature anomalies, with reference values (as used in Ludwigsen and Andersen (2020)) are 0 C° and 35psu, respectively. β is the saline contraction coefficient and α is the thermal expansion coefficient. The opposite sign of η_S is needed since β represents a contraction (opposite to thermal expansion). α and β are functions of absolute salinity, conservative temperature and pressure, and is determined with help from the freely available TEOS-10 software (Roquet et al., 2015). Map of $\dot{\eta}_S$ and $\dot{\eta}_T$ Sea level trends of η_S and η_T from 1995-2015 is are shown in figure 3.

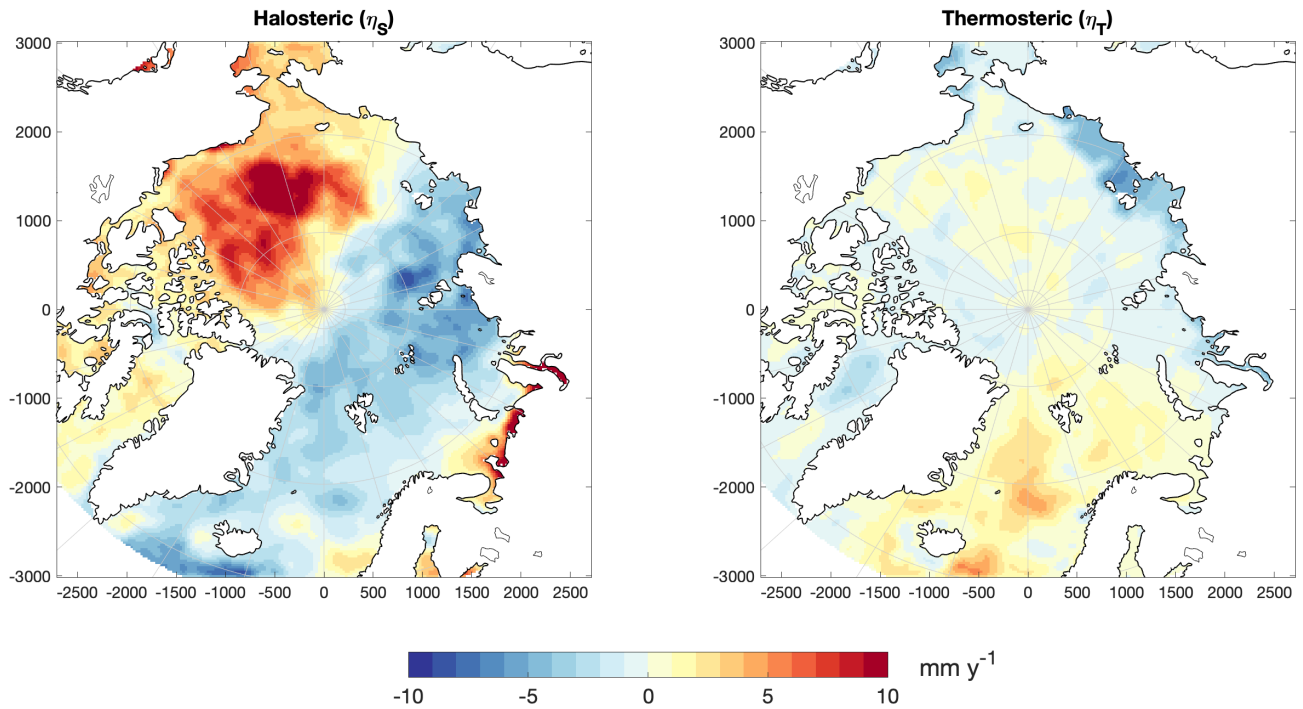


Figure 3. Halo- and thermosteric sea level trend [mm y^{-1}] from 1995-2015 derived from the DTU [Steric sea level](#) product ~~which was~~ used in Ludwigsen and Andersen (2020).

4 Mass contribution

3.1 [Manometric sea level contributions](#)

200 Maps of the individual contributions ~~to change in ocean mass is~~ [\(from equation 4\) to changes in manometric sea level](#) are shown in figure 4. ~~We divide the mass contributions into changes caused by changes in surface loading \dot{N} , from Greenland \dot{N}_{GRE} , Northern Hemisphere glaciers \dot{N}_{GNH} , Antarctica \dot{N}_{ANT} and GIA \dot{N}_{GIA} , and atmospheric pressure (IB) and a dynamic contribution ($D\dot{M}$).~~

$$\underline{\text{Mass}} = \dot{N}_{GRE} + \dot{N}_{GNH} + \dot{N}_{ANT} + \dot{N}_{GIA} + IB + D\dot{M}$$

205 Similar to the VLM-product (Ludwigsen et al., 2020a), the Regional Elastic Rebound Calculator (REAR) (Melini et al., 2015) ~~is used to estimate elastic gravitational changes.~~ [The gravitational change \(\$\dot{G}\$, while gravitational changes\)](#) of contemporary

changes in ice loading (equation 4) is (similar to the elastic VLM-component) computed using the elastic greens functions by REAR (Melini et al., 2015). The gravitational change from GIA is derived from the Caron2018-model. \dot{N} The sea level fingerprint (figure 4a-d) is retrieved by adding the spatially invariant constant c to the change of the geoid, \dot{G} ,

$$210 \quad \dot{N} = \dot{G} + c$$

c (barystatic sea level change) to the gravitational change and is equal to the contribution to global mean sea level (Spada, 2017), and. Following Spada (2017), c is defined as

$$c_i = -\frac{M_I \rho_w}{A_O} \frac{M_i \rho_w}{A_O} - \langle G_i - U_{VLM_i} \rangle \quad (10)$$

The used ice model with mass M_I , is a combined high resolution model for glacial estimates (Marzeion et al., 2012; Ludwigsen et al., 2017) and Greenland ice caps and is here an extended version of the model used for calculations of VLM, U , in (Ludwigsen et al., 2020a) where M_i is the mass change of the ice model, A_O is the global area of the ocean, while total ocean area, ρ_w is the average density of ocean water and $\langle \dots \rangle$, denotes the average of the ocean surface.

The geoid perturbation of non-tidal ocean loading (NOL) (van Dam et al., 2012) and rotational feedback (RF) (King et al., 2012) is not shown since it is below 0.05 mm. For calculating c_i , G_i and VLM_i for glaciers with REAR, individual glacial mass estimates are combined into a high resolution model for ice height change (Marzeion et al., 2012; Ludwigsen et al., 2020a). These estimated are combined with ice models for Greenland (Khan et al., 2016) and Antarctica (Schröder et al., 2019). From 1995 to 2015, the estimated ice loss is 142 Gt y^{-1} for Greenland, 206 Gt y^{-1} for Northern Hemisphere glaciers and 105 Gt y^{-1} for Antarctica and Southern Hemisphere glaciers, consistent with recent studies by Zemp et al. (2019); Shepherd et al. (2018, 2020)

225 The contemporary change in ice mass, M_i , but is included in \dot{N}_{GNH} . The change in surface mass, M_I , is zero for GIA, RF and NOL. The GIA contribution to global mean sea level (hence the barystatic GIA contribution defined from the right part of equation 10. c) for GIA is 0.3 mm y^{-1} consistent with other studies (Peltier, 2009; Spada, 2017). The gravitational change of RF and NOL (<0.05 mm y^{-1}) are included in the Northern Hemisphere glacial contribution to G .

230 Mass contributions to Arctic Sea Level mm y^{-1} from 1995-2015. The top four maps shows the geoid perturbations (\dot{N}) due to changes in surface mass loading or ocean bottom changes. Third row left is the sum of the top four maps. Right is atmospheric loading or Inverse Barometer (IB). Bottom left is the modeled ocean bottom pressure from ECCO and left is the difference between OBP and \dot{N} + atm. loading from third row.

Inverse Barometer (IB) The manometric sea level change is completed with the loading from atmospheric pressure, IB (figure 4e). IB is estimated by the simple relationship derived from the hydro-static equation (Naeije et al., 2000; Pugh and Woodworth, 2014). Monthly averaged pressure estimates from National Center for Environmental Prediction (NCEP) are used for the change in surface pressure surface pressure change Δp :

$$IB = -9.948 [\text{mm/mbar}] \Delta p \quad (11)$$

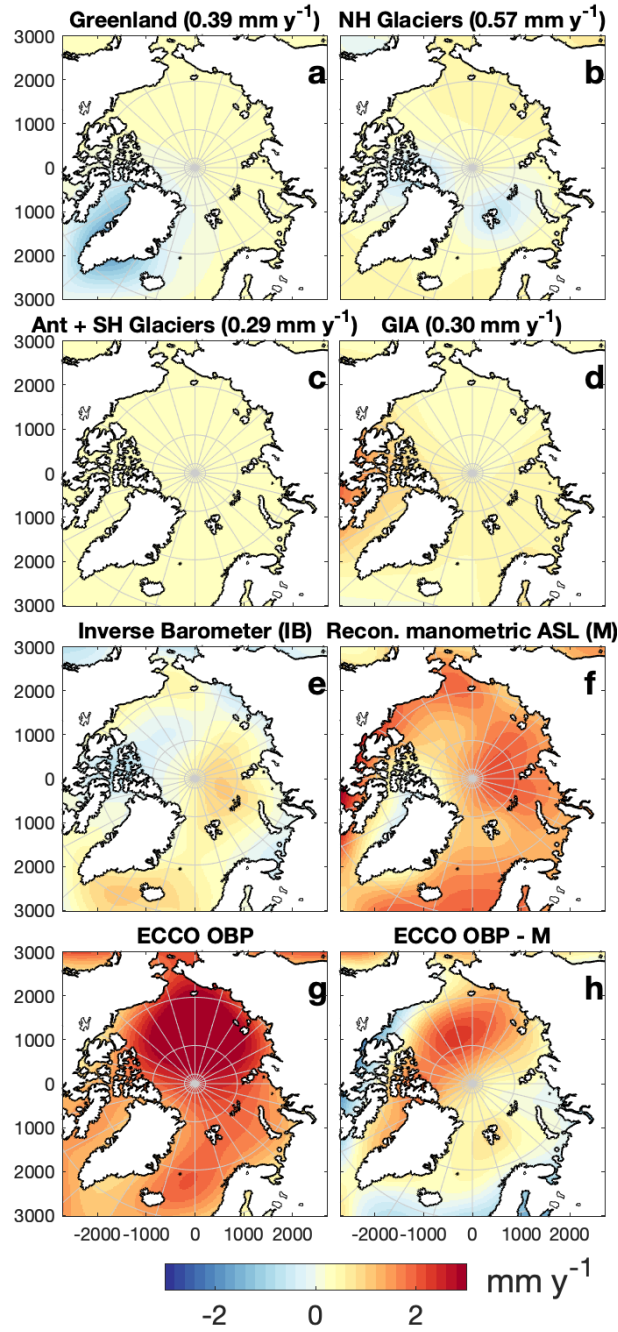


Figure 4. Contributions to the Arctic manometric sea level trend [mm y^{-1}] from 1995-2015. a-d shows \dot{N} (eq. 4) for different sources of land-to-ocean mass changes with the barystatic sea level contribution (\dot{c}) written in brackets: Greenland (incl. pherical glaciers) (a), Northern Hemisphere (NH) glaciers (b), Antarctica (Ant) + Southern Hemisphere (SH) glaciers (c), and GIA (d). The estimated Inverse Barometer trend (e). The sum of a-e and hence the total reconstructed manometric sea level trend (f). Modelled OBP-estimate from ECCOv4r4 (Fukumori et al., 2019) (g). Difference between g and f (h).

Figure 4 also shows the mass-trends derived from The total manometric sea level change (\dot{M} , figure 4f) is reconstructed as:

$$\dot{M} = \dot{N}_{\text{NHG}} + \dot{N}_{\text{GRE}} + \dot{N}_{\text{SH}} + \dot{N}_{\text{GIA}} + \dot{I}\dot{B} \quad (12)$$

240 Figure 4g shows the OBP-trend from the ECCOv4r4-model (Estimating the Circulation and Climate of the Ocean (ECCO) version 4 release 4) (Forget et al., 2015; Fukumori et al., 2019), which is used to estimate the dynamic contribution to sea level. The dynamic mass change is mainly a wind-driven effect that significantly changes the spatial distribution of ocean mass (Calafat et al., 2012; Dangendorf et al., 2014; Armitage et al., 2018) – also on secular time scales. a model estimate of \dot{M} . The difference between ECCO and \dot{M} is displayed in 4h.

245 Because the ECCO-model is among other forced by wind (Forget et al., 2015), we use the difference between ECCO and

4 Results

Generally, the steric (in particular the halosteric) sea level trend is dominating the spatial variability of the sum of \dot{N} and $\dot{I}\dot{B}$ as an estimate of the dynamic contribution to mass ($D\dot{M}$, bottom right map of figure 4) reconstructed sea level trend (ASL_r), with over 10 mm y^{-1} in the Beaufort Gyre and -7 mm y^{-1} in the Russian Arctic (figure 3).

250 5 Comparison of estimates of the Arctic Absolute Sea Level Trend

Two derived trend estimates of the ASL budget is created from steric + mass ($\dot{\eta} + \dot{N} + \dot{I}\dot{B}$) (without the dynamic component) and steric + mass (ECCO), where ECCO is used as the mass component and hence includes dynamic mass changes. In contrast, is the reconstructed manometric sea level trend (\dot{M}) varying between 0 and 2 mm y^{-1} , with smaller spatial variability. This is in alignment with the 2003–2015 OBP-estimates from GRACE JPL mascons (Wiese et al., 2016) used in Ludwigsen and Andersen (2020) but way smaller than the estimates from GSFC mascons (Luthcke et al., 2013) used by Raj et al. (2020) and CSR (Save et al., 2016) used by Carret et al. (2017).

260 Figure 4a-c shows that the contributions from contemporary ice loading has a (compared to steric) small contribution to spatial sea level variability, but the sea level fingerprints from deglaciation of Greenland and glaciers are however til clearly visible with a absolute sea level fall of 0.5 to 1 mm y^{-1} , which seems to be in agreement with global sea level fingerprint studies of Bamber and Riva (2010); Spada (2017); Frederikse et al. (2018). In total, the three figures sums to a sea level rise of around 1 mm y^{-1} in most of the Arctic, except close to areas with deglaciation (like Greenland and Svalbard). They are compared to the independent estimates of ASL change from TG corrected for VLM and altimetry

Figure 4g shows that ECCO has a higher manometric sea level change in the interior of the Arctic Ocean, while the coastal zones, except east Siberia, are lower than \dot{M} .

265 The two derived ASL-trend estimates are shown. ECCO-model does attempt to include term dynamic sea level changes associated with wind-forcing and ocean currents into their OBP-estimate (Forget et al., 2015). Those changes are not part of \dot{M} and is probably the main reason for the difference between ECCO OPB and \dot{M} .

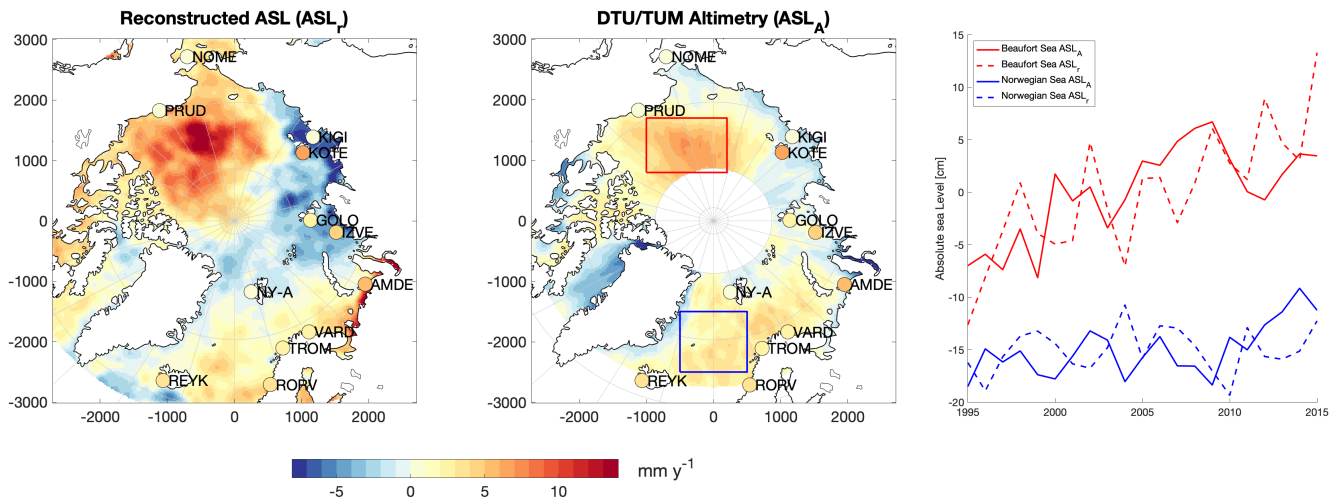


Figure 5. Absolute sea level trend of the reconstructed product (ASL_r) (left) and from 1995-2015 DTU/TUM Altimetry (ASL_A) (middle) from 1995 to 2015 [$mm\ y^{-1}$]. Left shows perturbation of the geoid + steric contribution, in the middle is OBP from ECCO combined with steric and right is altimetric sea level from Rose et al. (2019). The circles indicate show the absolute sea level trend of the 12 VLM-corrected tide gauges (ASL_{TG}). Right plot shows timeseries of ASL_A and ASL_r for two selected areas (marked in the DTU/TUM Altimetry map).

4.1 Comparing reconstructed ASL with altimetry

The reconstructed ASL (ASL_r) trend is compared to the altimetric ASL trend (ASL_A) in figure 5. Since ECCO is partly assimilated with altimetry, only the mass contribution without the dynamic component is truly independent from altimetry. On the scale shown in figure 5, we see that the differences are hardly recognizable, while TG-based ASL (ASL_{TG} trend is indicated with dots. Table 1 and figure 6 shows the sea level contributions estimated at each tide gauge. There is an overall agreement of the sea level trend pattern in both ASL_r and ASL_A . The main obvious difference between the spatial sea level pattern of ASL_r and ASL_A is the larger sea level rise in the Beaufort Sea and sea level fall in the East-Siberian seas of ASL_r .

Because of Before the era of SAR altimetry (from October 2010), the ability to separate the leads and the sea ice was more difficult due to the larger footprint of the conventional satellites. Therefore, in areas with a dense sea ice cover (like the Beaufort Sea), more altimetric observations exist during the sea level high of the autumn and fewer during winter/spring where sea level is lower (i.e. Armitage et al. (2016)). This creates a seasonal bias that is more pronounced before the sea-ice bias before the launch of CryoSat-2 in end-2010, CryoSat-2 era, because of the lower resolution in the values before 2011 are likely to be overestimated, which results in a pre-SAR era. This bias can explain the 'flattening' of the trend. In particular, this seems to be the case in the Beaufort Sea (see seen in figure 5), where altimetry and the derived mass+steric product agree on the spatial extent of the doming of the Beaufort Gyre, but altimetry is $-5\ mm\ y^{-1}$ lower than the mass + steric estimate. ASL_A shows a smaller doming of the Beaufort Gyre than ASL_r . From the time series (right panel of figure 5) is it evident that ASL_A is higher than ASL_r from 2003-2009 and then shifts to a lower level after 2010. The same difference between ASL_r and ASL_A is not

285 observed in a predominately non-SAR region of the Norwegian Sea. Another altimetry ~~product from Armitage et al. (2016)~~
~~has based SLA-estimate from 2003-2015 (Armitage et al., 2016)~~, observes a larger trend in the Beaufort Gyre in alignment
with the ~~steric+mass products~~ values of ASL_r .

~~1995-2015 sea level trends $mm\ y^{-1}$ of each contribution at the 12 tide gauge locations. The values (except VLM) represent a
100 km radius around the tide gauge. For VLM a 5 km radius is used and for Ny-Ålesund and Reykjavik, VLM is taken from~~
290 ~~GNSS. The columns in bold indicate the estimates of Absolute Sea Level (ASL).~~

~~Components of sea level trend $mm\ y^{-1}$ for each tide gauge from 1995-2015. The three bars in the middle (Steric+geoid+dyn,
ASL (altimetry) and ASL (tide gauge)) are independent estimates of absolute sea level. The errorbars indicate one standard
error (combined error from each component when relevant). The VLM component 'Local (GNSS-VLM)' is only relevant at
Reykjavik and Ny-Ålesund, because significant local properties causes VLM that is not present in the VLM-model (Ludwigsen et al., 2020b)~~
295 ~~-. Glacier component of VLM includes the effect of rotational feedback, ocean loading, and Antarctica which are less than 0.5
 $mm\ y^{-1}$ combined.~~

In the altimetric ~~product estimate (middle panel of figure 5)~~ a positive sea level trend extends in the Norwegian Sea until it
reaches the average sea ice boundary, which (intentionally) coincides with the SAR-boundary of CryoSat-2. From altimetry it
is unclear if this signal is a real physical signal or due to bias when different ~~satellites and altimetric observations (different~~
300 ~~satellites and SAR/non-SAR)~~, sea ice and open ocean regions are aligned in the DTU/TUM product ~~-. We see from the derived
mass+steric product, that or an error in the SAR-based DTU18MSS (Andersen et al., 2018) that is used as a reference in the
altimetry data. From the ASL_r , some of the positive sea level trends are is restored in the Norwegian Sea by a combination of
the thermosteric contribution (figure 3) , -thus is a warming of the ocean cause to sea level rise in the region and the negative
gravitational contribution from Greenland (figure 4a). The boundary between sea ice and open ocean is however less significant~~
305 ~~in ASL_r and a spatial bias in altimetry cannot be excluded.~~

~~Obviously, does tide gauges-~~

4.2 Comparing ASL-trends at tide gauge locations

TGs only measure sea level in coastal areas, and are therefore not useful when analyzing spatial sea level trend patterns of the
Arctic Ocean. Furthermore, is the coastal location often disturbed by the local environment that might be unknown (e.g. small
310 river outflow, local construction, packing of sea ice etc.), which can influence both sea level measurements from tide gauge and
altimetry.

In figure 6 and table 1, ~~we quantify~~ the contributions to ~~sea level change explained in this chapter at~~ ASL_r is quantified at the
location at each of the ~~12 tide gauge locations using a surrounding average of 100 km radius twelve TGs by taking the mean
trend of a radius of 50 km~~ (5 km for GIA and elastic VLM). This radius ensures, that Rorvik, Nome and Reykjavik ~~reaches~~
315 ~~overlaps~~ the altimetric data, but ~~few data points, the fewer number of data points~~ might cause the data to be more variable and
hence increase the uncertainty (estimated as standard error, σ).

The Norwegian tide gauges (Rorvik, Tromso, Vardo) are considered the most stable ~~-. The derived product and also show
the lowest error estimate (together with Ny-Ålesund).~~ ASL_r is in good agreement with the tide gauge and has for Tromso and

	\dot{RSL}_{TG}	VLM (model/GNSS)	\dot{ASL}_{TG}	IB	\dot{N}	\dot{M}	$\dot{\eta} (\eta_S + \eta_T)$	\dot{ASL}_r	\dot{ASL}_A
NOME	2.0 ± 9.0	-1.1 ± 0.9	0.9 ± 9.1	0.1	1.1 ± 0.7	1.2 ± 0.7	1.7 ± 12.9	2.8 ± 12.9	0.2 ± 4.9
PRUDHOE BAY	1.7 ± 7.4	-1.4 ± 1.3	0.4 ± 7.5	0.4	1.0 ± 0.9	1.4 ± 0.9	5.7 ± 14.2	7.1 ± 14.2	1.1 ± 5.2
REYKJAVIK	3.8 ± 3.1	0.0 ± 0.3	3.8 ± 3.1	1.0	0.3 ± 1.5	1.3 ± 1.5	-0.4 ± 2.8	0.9 ± 3.1	2.3 ± 2.8
RORVIK	-0.7 ± 5.1	4.3 ± 1.8	3.6 ± 5.4	0.3	1.3 ± 0.7	1.5 ± 0.7	2.0 ± 5.2	3.5 ± 5.3	2.4 ± 2.4
NY-ALESUND	-7.4 ± 3.7	8.0 ± 0.5	0.5 ± 3.7	0.6	0.1 ± 3.4	0.7 ± 3.4	-2.0 ± 2.2	-1.3 ± 4.0	1.1 ± 1.4
TROMSO	-0.1 ± 4.1	2.3 ± 1.7	2.2 ± 4.4	0.1	1.1 ± 0.9	1.3 ± 0.9	-0.1 ± 1.9	1.2 ± 2.1	2.2 ± 1.9
VARDO	-0.0 ± 3.8	2.5 ± 1.4	2.5 ± 4.0	-0.1	1.2 ± 0.9	1.1 ± 0.9	0.6 ± 3.2	1.7 ± 3.3	4.1 ± 1.9
AMDERMA	4.9 ± 4.7	0.2 ± 1.1	5.1 ± 4.9	-0.1	1.1 ± 0.8	1.0 ± 0.8	3.9 ± 11.1	4.9 ± 11.2	-0.8 ± 4.5
IZVESTIA TSIK	2.7 ± 4.6	2.3 ± 1.5	5.0 ± 4.8	0.2	1.1 ± 1.1	1.3 ± 1.1	-5.2 ± 8.0	-3.9 ± 8.0	1.0 ± 5.5
GOLOMIANYI	0.0 ± 3.5	2.8 ± 2.3	2.8 ± 4.2	0.6	0.9 ± 2.1	1.5 ± 2.1	-5.4 ± 7.9	-3.9 ± 8.2	-0.7 ± 6.0
KOTELNYI	7.7 ± 5.4	-1.1 ± 0.8	6.5 ± 5.4	0.2	1.1 ± 0.7	1.4 ± 0.7	-7.5 ± 15.3	-6.1 ± 15.3	-0.8 ± 5.7
KIGILIAH	1.7 ± 4.8	-0.9 ± 0.7	0.8 ± 4.9	-0.1	1.2 ± 0.7	1.0 ± 0.7	-7.9 ± 14.8	-6.8 ± 14.8	-1.6 ± 5.1

Table 1. 1995-2015 sea level trends [mm y^{-1}] at the 12 tide gauge locations. The trends (least-squares) are generally based on an annual mean-value of a 50 km radius around the tide gauge. For VLM a 5 km radius is used, except for Ny-Alesund and Reykjavik where VLM is based on GNSS-measurements. The columns in bold indicate the three estimates of Absolute Sea Level (\dot{ASL}_{TG} , \dot{ASL}_r and \dot{ASL}_A).

~~Vardo is for Rorvik and Vardo in~~ better alignment with ~~the TG-data than altimetry~~ \dot{ASL}_{TG} than \dot{ASL}_A . This is also the region with highest density of hydrographical data and thus ~~most reliable~~ the region with the most reliable steric estimate. We see that for Vardo and Rorvik, the sea level change is split between a steric and a mass contribution of roughly the same size, which is similar to the share of the global sea level trend (Church and White, 2011b; WCRP, 2018). At Tromso a negative halosteric ~~signal trend~~ (more saline water) is lowering ~~the sea level trend~~. \dot{ASL}_r . However, \dot{ASL}_r around Tromso (50-200 km) yields a better agreement with the observed \dot{ASL}_{TG} and \dot{ASL}_A .

~~Along the Siberian coast,~~

~~The Siberian coast has~~ multiple river outlets ~~contributes to a freshening that contributes with freshwater~~ of the Arctic Ocean (Morison et al., 2012; Armitage et al., 2016), which is reflected by the ~~positive halosteric trend~~ (Proshutinsky et al., 2004; Morison et al., 2004). ~~A positive halosteric sea level trend is visible at the coast of the Bering and Kara Sea, where the river OB has a major outflow.~~ At Amderma TG, which is located on the coast between the Barents and Kara Sea, ~~there is however no nearby major river outlet, but but not near any major outflow,~~ a significant halosteric ~~signal is still present which matches the tide gauge measured sea level trend is recognized by the TG-measured sea level, despite rather large uncertainties~~. Ice loss from Novaya Zemlya contributes with over 1 gigaton of freshwater to the Kara Sea every year and the ice loss has been accelerating (Melkonian et al., 2016), but ~~it is unclear if this is the reason for the halosteric sea level rise at Anderma, or if the halosteric signal is the contribution is small compared to the +500 Gt coming from the rivers every year. The halosteric signal could (falsely) be~~ extrapolated from the gulf of Ob which has ~~major major~~ river outlets and the ~~match with tide gauge agreement with \dot{ASL}_{TG}~~ is accidental. ~~The altimetric signal reflects the mass contribution, which together with low hydrographic data density in the region, could indicate that both the tide gauge and~~ So the reason for this halosteric sea level ~~trends are overestimated. rise at~~

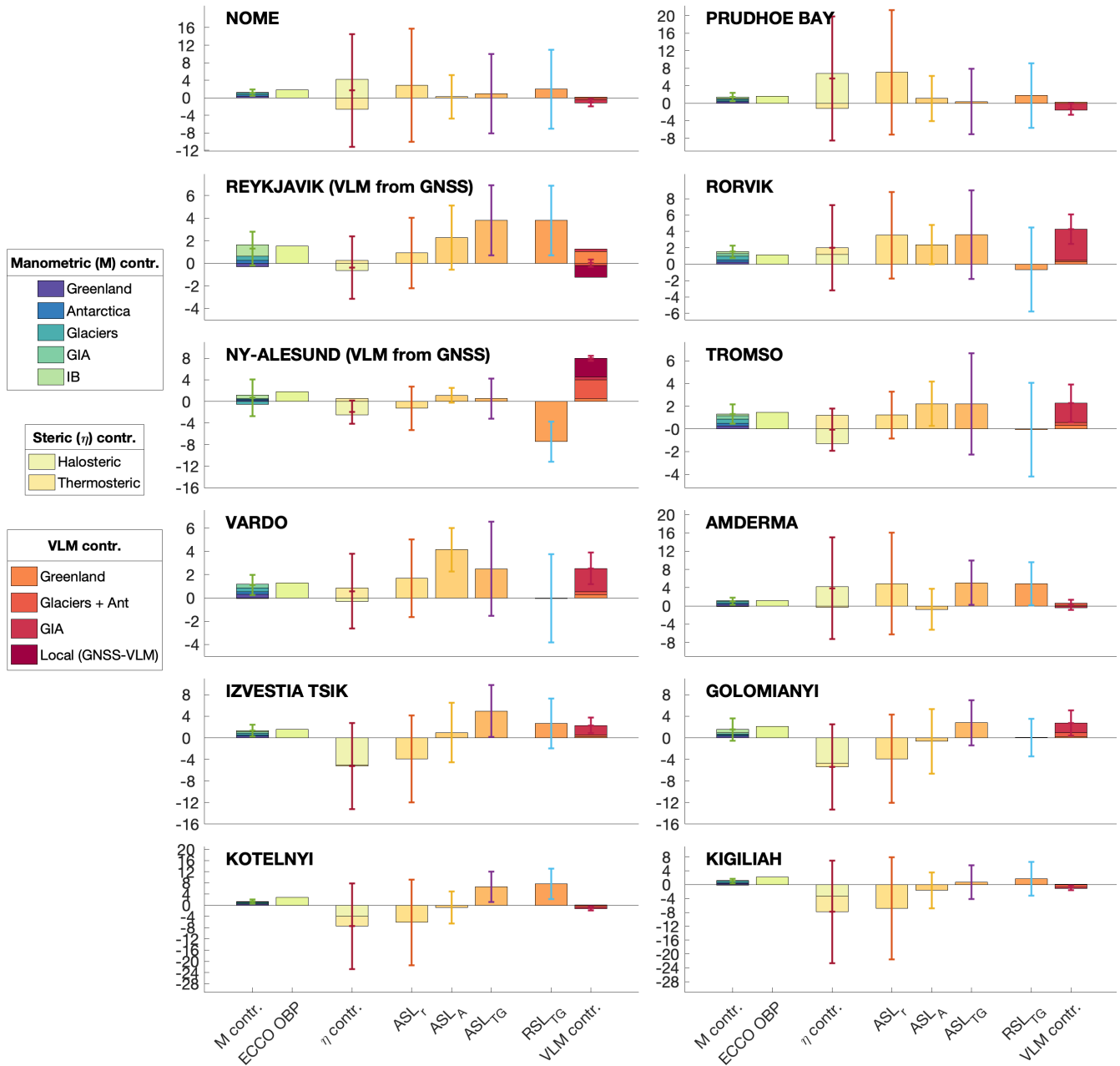


Figure 6. Components of sea level trend [mm y^{-1}] for each tide gauge from 1995-2015. The three bars in the middle (ASL_r , ASL_A and ASL_{Tg}) are the three independent estimates of absolute sea level. The error bars indicate one standard error (combined error from each component when relevant). The VLM component 'Local (GNSS-VLM)' is only relevant at Reykjavik and Ny Ålesund, because significant local properties causes VLM that is not present in the VLM-model (Ludwigsen et al., 2020b). Glacier component of VLM includes the effect of rotational feedback, ocean loading, and Antarctica which are less than 0.5 mm y^{-1} combined.

Anderma is remains unclear. In any case, both ASL_{TG} and ASL_r is in opposition to altimetry observations that shows a negative ASL -trend.

340 ~~The four other tide gauges~~ Further east along the Siberian coast the four TGs (Izvestia Tsik, Golomianyi, Kotelnyi, Kigiliah) all show a ~~pattern, where mass+steric has rising ASL , while both ASL_A and in particular ASL_r shows a negative trend ; altimetry has a slight negative or positive trend and the tide gauge has a clear positive trend.~~ Due to in the region. Even though the ECCO OBP is $1-2 \text{ mm y}^{-1}$ higher than the manometric estimate (figure 4) it is not enough to explain the discrepancy between ASL_{TG} and ASL_r , but explains some of the ASL_A/ASL_r difference. Figure 3 shows that a negative halosteric sea
345 level trend is dominating the reconstructed sea level trend in the region, but the poor hydrographic coverage along the Siberian coast (Ludwigsen and Andersen, 2020) ~~it is difficult to estimate the 'true' sea level.~~ The positive makes the uncertainty of the halosteric trend large. This negative steric sea level trend is however supported by the results of Armitage and Davidson (2014) from combining GRACE with altimetry. They estimate a steric sea level in the Siberian Arctic (excluding the Barents Sea) in the order of -5 mm y^{-1} from 2003 to 2014, which is same order of the estimated steric trend of this study in the region.

350 The positive ASL trend among tide gauges in the Siberian Seas eastern Russian Arctic is however consistent and has been recognized in other studies using an extended set of Siberian-Russian tide gauges (Proshutinsky et al., 2004; Henry et al., 2012). Remarkably is that the TG-trend at Kotelnyi and Kigiliah differ with almost 6 mm y^{-1} (in total 12 cm difference over the time span of this study) despite being less than 250 km apart. This ~~difference is only realistic~~ gradient is only reasonable, if local circumstances is affecting the RSL, that affects the RSL is considered. Local coastal subsidence not associated with land
355 ice loss/gain, i.e. caused by thawing of permafrost or oil depletion, is a possible explanation.

Nome and Prudhoe Bay in Alaska both show a positive steric trend which is not reflected in sea level trends from altimetry or the tide gauge, thus resulting in a rather large discrepancy between ASL_r and ASL_{ATG} . The strong halosteric trend of the Beaufort Gyre, might be extrapolated towards the Alaskan coastline ~~Altimetry agrees reasonably well with the tide gauge trend.~~ and into the Bering Strait in the DTU steric model. There is no evidence in the literature for a extent of the Beaufort
360 Gyre doming as shown from the halosteric trend, which indicates, that the weighted spatial interpolation in combination with higher hydrographic data density in the Beaufort Sea creates this widening of the Beaufort Gyre.

~~Maps of uncertainty (1 standard error) of the 1995-2015 trend mm y^{-1} for combined steric, combined $\dot{N} + \text{dynamic mass} + \text{IB}$, altimetry and combined VLM contributions. Few hydrographic data around Reykjavik, makes the steric sea level rather uncertain as well. A negative halosteric contribution causes the steric+mass product to be to low compared to TG-data and altimetry.~~

365 ~~altimetry.~~

~~At Ny-Ålesund on Svalbard, which like the other Norwegian TG-sites has good hydrographic data density, is the mass + steric contribution in agreement with the TG-trend. Ny-Ålesund on Svalbard is dominated by a large VLM caused by deglaciation in recent years and after the Little Ice Age that ended in the 19th century (Rajner, 2018; Ludwigsen et al., 2020a) recent deglaciation. This uplift completely mitigates the large sea level fall measured by the tide gauge. A small mass upward trend is countered by a smaller steric downward trend, which in total agrees with the tide gauge measured sea level trend. Altimetry shows a slightly higher trend, and results in small rise of ASL_{TG} . In (Ludwigsen et al., 2020a) it is argued that the discrepancy between GNSS and the VLM-model in large originates from VLM because of post-LIA deglaciation on~~

370 ~~altimetry shows a slightly higher trend, and results in small rise of ASL_{TG} . In (Ludwigsen et al., 2020a) it is argued that the discrepancy between GNSS and the VLM-model in large originates from VLM because of post-LIA deglaciation on~~

Svalbard (Rajner, 2018). This viscoelastic GIA-like LIA-effect will certainly also have a gravitational sea level fingerprint (\dot{N}) that should be added to the manometric sea level change \dot{M} . This can explain some of the difference between ASL_T and $ASL_{A/TG}$. A possibly positive dynamic \dot{M} -change (from the (ECCO OBP)– \dot{M} difference in figure 4h) could further close the ASL_T – $ASL_{A/TG}$ gap.

From the calculations of the gravitational fingerprint, none of the TG-sites in this study experience a net sea level fall from contemporary deglaciation and GIA (\dot{N} in table 1) and only Ny-Ålesund (-0.4 mm y^{-1}) and Reykjavik (-0.2 mm y^{-1}) will experience a small sea level fall from contemporary deglaciation alone. So even though the Arctic is heavily prone to ice mass loss and thus a smaller gravitational pull, the Arctic as a region is not experiencing a absolute sea level fall from contemporary deglaciation. On the contrary, it causes the sea level to rise with around 1 mm y^{-1} in most of the Arctic. However, by accounting for the deglaciation effect on VLM, the RSL-change from contemporary deglaciation will be negative in large areas of the Arctic.

5 Uncertainty and assessment of ASL-trends

The uncertainties of the trend estimates for RSL_{TG} , VLM, gravitational fingerprint (N), steric (η) in table 1 and figure 6 are derived as the standard error (σ) of the detrended timeseries of the annual mean values. GIA (Caron et al., 2018) and altimetry (Rose et al., 2019) has a associated uncertainty that is used. In the case of VLM a 10% error is added to account for uncertainties of the earth model (Wang et al., 2012).

Generally The spatial distribution of the uncertainties are shown in figure 7. Generally, the largest uncertainties (~~estimated as standard error of the trend~~) are found along the Siberian coast and in the interior of the Arctic where the largest sea level trend is present (see figure 7). The steric uncertainty, ~~which is~~ in most cases ~~is~~ the largest source of uncertainty, ~~is computed as the standard deviation of the detrended and deseasoned time series, which~~ (figure 6). The standard error naturally reflects if ~~the~~ steric heights are unstable and poorly constrained. ~~This method requires in principal~~ (if for example there are few hydro-graphic data). In principle, this method requires temporal independence, which is not entirely true, since ~~outliers are replaced with~~ data from adjacent years ~~are used instead of outliers~~. Furthermore, large influence by the non-periodic and non-linear Arctic Oscillation, would enhance the uncertainty, even though this is a real physical signal. ~~Thereby is the estimated error a composite of uncertainties originating from the way the sea level component is constructed and from, the sometimes large, interannual variability.~~

The mass contribution and VLM has naturally the largest uncertainties close to glaciated areas. Glacial ice loss on Baffin Island is poorly constrained in the ice model, which is reflected ~~in with~~ large uncertainties in this area. ~~A significant uncertainty also originates in the dynamic mass loss, which probably also can be attributed to the Arctic Oscillation, which significantly changes wind patterns. Since no uncertainties are associated with the ECCO-product, we also here assume no temporal correlation, and calculate the standard deviation of the time series, even though the model likely has inter-annual correlations. The uncertainty of altimetry is reflecting the data availability of areas with sea ice contrary the ice-free ocean, while the largest uncertainties of the TGs are those with largest interannual variability.~~

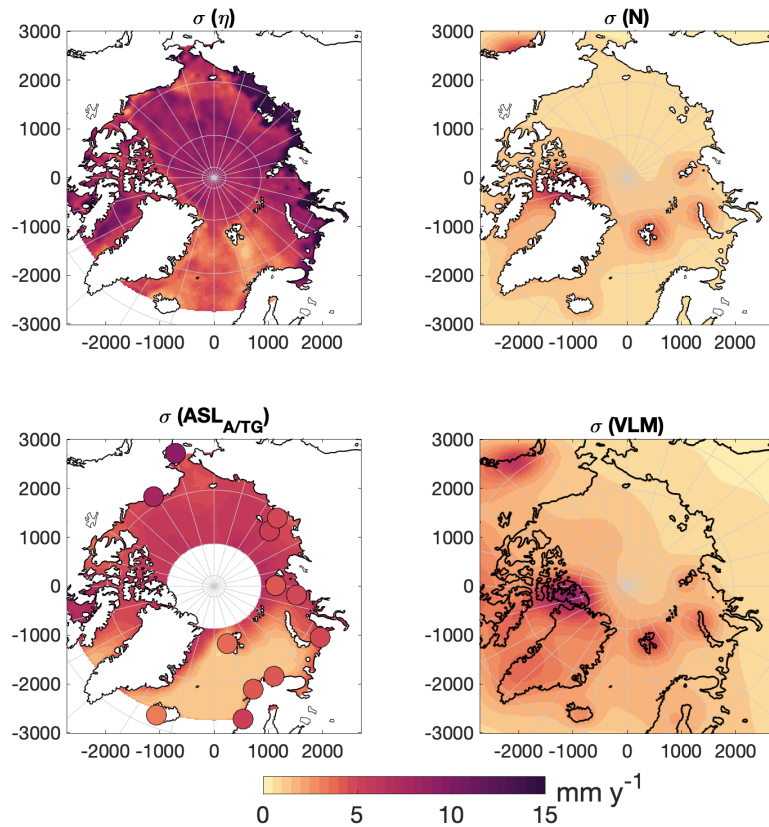


Figure 7. Map in the top row shows the absolute difference between altimetry and the steric+mass Standard error (no dynamic contribution) σ product (left column) and altimetry and of the 1995-2015 trend [mm y^{-1}] for combined steric+mass from the ECCO-model (right column). Bottom row, shows the absolute difference relative to the combined uncertainty (σ). The dots show the difference to VLM-corrected tide gauges. At the tide gauges marked with black \bar{N} , is the difference larger than the ASL_{ATG} and combined uncertainty VLM contributions.

410 Left map of figure 8 shows the difference between ASL_r and ASL_{ATG} . The pattern somehow resembles the trend of the halosteric contribution, which reflects the halosteric dominance of the spatial variability. The correlation coefficient (R) between ASL_r and ASL_A is $R=0.50$ ($R=0.23$ without the halosteric contribution) and $R=0.53$ when using the ECCO OBP estimate instead of the reconstructed manometric sea level. The correlation is better than the correlation coefficients reached by (Ludwigsen and Andersen, 2020), where they used different datasets of GRACE ($R=0.19-0.40$) combined with the same steric and altimetric datasets. From the middle panel in figure 8 we see that for most of the Arctic (78%) and for 8 of 12 TGs, the absolute difference is less than half of the combined standard error and in 98% of the area, is ASL_r in agreement with ASL_A within the associated uncertainty, which indicates that the error is a conservative estimate. Only the TG Izvestia Tsik shows a larger difference between observed (ASL_{TG}) and reconstructed sea level (ASL_r) than the associated standard error.

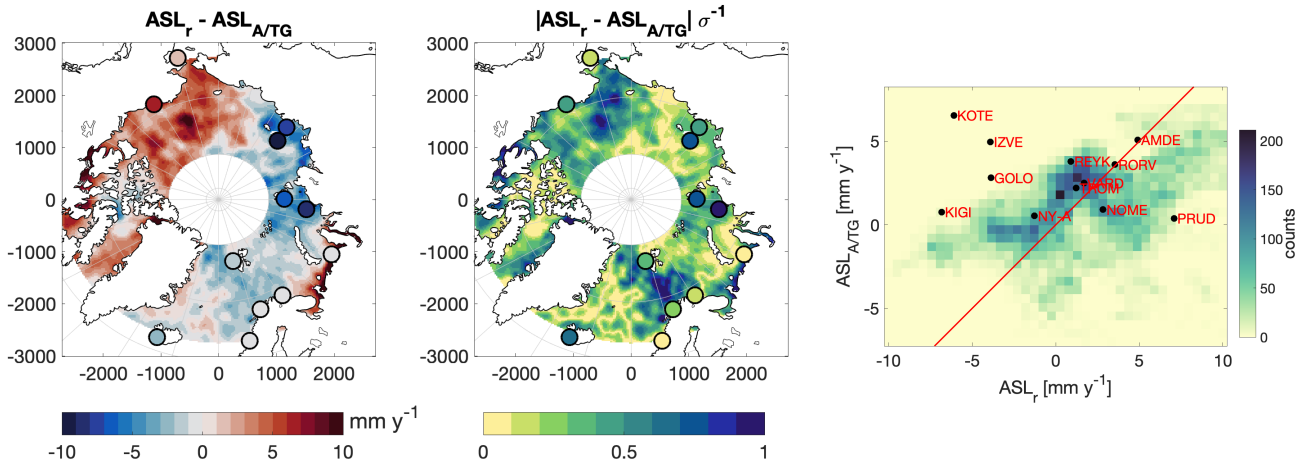


Figure 8. Left map shows the difference between ASL_r and $ASL_{A/TG}$. Middle map is the absolute difference divided by the standard error from 7 (combined uncertainty). Right panel shows a correlation matrix between ASL_r and $ASL_{A/TG}$. The color indicates the number of data grid cells falling into bin size of 0.5 mm y^{-1} . 96% of the grid cells with data is covered within the bounds of the matrix ($N_{\text{total}}=18150$). The red line is where ASL_r is equal to $ASL_{A/TG}$.

415 The right panel of figure 8 shows the correlation matrix between observed ASL ($ASL_{A/TG}$) and reconstructed ASL (ASL_r). The matrix shows that ASL_r and ASL_A are largely correlated. There is large accumulation around 2 mm y^{-1} , with slightly higher ASL_A than ASL_r . This originates from the underestimate of the ASL-reconstruction (see figure 8) in the Norwegian Sea and the difference agrees with the ECCO OBP-M difference (figure 4h) and thus likely explained by the missing dynamic sea level contribution of M. Evident are also the large positive ASL_r -trends from the Beaufort Sea and negative ASL_r -trends
 420 along the Siberian Coast that is not reflected in ASL_A .

6 Conclusion

All significant contributions to the sea level change from 1995-2015 in the Arctic Ocean ~~have been were~~ mapped and assessed at 12 tide gauges located throughout the Arctic Ocean. This was done for the first time without the use of GRACE data or modeled steric data. Thereby are we able to ~~attribute effects on Arctic Sea Level~~ reconstruct the Arctic absolute sea level
 425 ~~change and attribute the changes~~ to their origin and thus understand the causes behind the ~~observed altimetry and TG-observed~~ sea level trend. By using a VLM-model, that includes both GIA and elastic uplift, the ~~TG-data~~ TG-observed sea level can be utilized in locations ~~if where~~ no reliable GNSS-data is present.

From figure 5 we clearly see that the general spatial pattern of altimetry ~~observed sea level~~ (ASL_A) is restored in the ~~derived steric estimate and in the mass product~~ reconstructed ASL-estimate (ASL_r). The correlation ($R=0.50$) outperforms

430 GRACE-based sea level budget assessments from (Ludwigsen and Andersen, 2020) (R=0.19-0.40). Figure 6 and 7 ~~shows show~~ that steric sea level dominates the spatial variability ~~and~~. This is also the main source of uncertainty, while manometric sea level change has a more uniform and smaller contribution to ASL. Some areas, in particular, the Norwegian Sea ~~and more interior of the Arctic Ocean, seems to be rather well constrained and understood from~~, has more observations (from both altimetry and hydrographic data) and thus can the individual contributions be estimated with lower uncertainty. The Siberian ~~seas, Seas~~ are however poorly constrained with observations and both the steric product, altimetry and tide gauges show large ~~uncertainty uncertainties~~. Figure 8 shows the spatial agreement between ~~altimetry/tide gauges and the steric+mass or steric+mass(ECCO) product~~ observed sea level (ASL_{A/TG}) and the reconstructed ASL estimate within the combined uncertainty. ~~Without the use of ECCO, the derived product~~ The reconstructed ASL-estimate agrees with altimetry at in 98% of the area ~~, while only 5 out of 12 of the TG-data agree with derived product. For the steric+mass(ECCO) product, the products~~ agree at 99% of the area and at and 11 out of of the 12 TG's. ~~The areas of disagreement in the Norwegian Sea can be explained by the very low altimetric uncertainty in the area~~ TGs within the uncertainty.

~~Our results show~~ The correlation between the reconstructed sea level and altimetry is significant (R=0.50), but also shows that the sea level budget is not closed or completely understood everywhere in the Arctic - likely because of poorly constrained steric data and a uncertain dynamic contribution ~~, however, from~~ that is difficult to reconstruct. However, the reconstructed sea level confirms the negative halosteric-driven sea level trend along the east Siberian coast identified by (Armitage and Davidson, 2014) , which is in contrast to the TG-observed sea level in the region. Large variations among TGs in East Siberia indicate very local VLM affecting the TG-observed RSL.

From figure 8 we see that the uncertainties ~~are~~ in most of the Arctic are significantly larger than the difference between ~~a derived product and altimetry, the reconstructed sea level and altimetry. This is~~ including most of the Siberian Seas. ~~More precise~~, indicating that the uncertainty of the components of this study of the sea level trend might be a conservative estimate. Better constrained estimates of both the ~~mass and steric product~~ manometric and steric sea level are necessary to get at a complete understanding of what changes Arctic sea level and to validate sea level trends observed by altimetry, which ~~is~~ are not necessarily more accurate than the derived ASL-estimates.

Code and data availability. Tide gauge sea level timeseries is available at psmsl.org, the VLM-model available at data.dtu.dk/articles/dataset/Arctic_Vertical_Land_Motion_5x5_km, DTU Steric is available at ftp.space.dtu.dk/pub/DTU19/STERIC/, the REAR-software is available at github at github.com/danielemelini/rear.git.

Author contributions. CAL: Method, concept, data analysis and writing. OBA: Concept and editing. SKR: Providing altimetry data, validation and editing.

Competing interests. The authors declare no competing interests.

460 *Acknowledgements.* The authors want to thank two anonymous reviewers for their comments that greatly improved the manuscript. Furthermore, we thank Lambert Caron for ~~creating~~ providing the Caron2018 GIA-model, available at <https://vesl.jpl.nasa.gov/solid-earth/gia/> ~~-Special thanks to~~ and Danielle Melini for creating the REAR-code (Melini et al., 2015). This research was funded by the EU-INTAROS project (Grant agreement no. 727890) (CAL and OBA) and by the ESA-Climate Change Initiative Sea level budget closure (Expro RFP/3-14679/16/INB) (OBA and SKR).

465 References

- Andersen, O., Knudsen, P., and Stenseng, L.: A New DTU18 MSS Mean Sea Surface – Improvement from SAR Altimetry, p. 172, 25 years of progress in radar altimetry symposium ; Conference date: 24-09-2018 Through 29-09-2018, 2018.
- Armitage, T. W. K. and Davidson, M. W. J.: Using the Interferometric Capabilities of the ESA CryoSat-2 Mission to Improve the Accuracy of Sea Ice Freeboard Retrievals, *IEEE Transactions on Geoscience and Remote Sensing*, 52, 529–536, 2014.
- 470 Armitage, T. W. K., Bacon, S., Ridout, A. L., Thomas, S. F., Aksenov, Y., and Wingham, D. J.: Arctic sea surface height variability and change from satellite radar altimetry and GRACE, 2003–2014, *Journal of Geophysical Research: Oceans*, 121, 4303–4322, <https://doi.org/10.1002/2015JC011579>, <https://agupubs.onlinelibrary.wiley.com/doi/abs/10.1002/2015JC011579>, 2016.
- Armitage, T. W. K., Bacon, S., and Kwok, R.: Arctic Sea Level and Surface Circulation Response to the Arctic Oscillation, *Geophysical Research Letters*, 45, 6576–6584, <https://doi.org/10.1029/2018GL078386>, <https://agupubs.onlinelibrary.wiley.com/doi/abs/10.1029/2018GL078386>, 2018.
- 475 Bamber, J. and Riva, R.: The sea level fingerprint of recent ice mass fluxes, *The Cryosphere*, 4, 621–627, <https://doi.org/10.5194/tc-4-621-2010>, <https://www.the-cryosphere.net/4/621/2010/>, 2010.
- Behrendt, A., Sumata, H., Rabe, B., and Schauer, U.: A comprehensive, quality-controlled and up-to-date data set of temperature and salinity data for the Arctic Mediterranean Sea (Version 1.0), links to data files, <https://doi.org/10.1594/PANGAEA.872931>, <https://doi.org/10.1594/PANGAEA.872931>, supplement to: Behrendt, A et al. (2017): UDASH - Unified Database for Arctic and Subarctic Hydrography. *Earth System Science Data Discussions*, 37 pp, <https://doi.org/10.5194/essd-2017-92>, 2017.
- 480 Box, J. E., Colgan, W. T., Christensen, T. R., Schmidt, N. M., Lund, M., Parmentier, F. J. W., Brown, R., Bhatt, U. S., Euskirchen, E. S., Romanovsky, V. E., Walsh, J. E., Overland, J. E., Wang, M., Corell, R. W., Meier, W. N., Wouters, B., Mernild, S., Mård, J., Pawlak, J., and Olsen, M. S.: Key indicators of Arctic climate change: 1971–2017, *Environmental Research Letters*, 14, 045 010, <https://doi.org/10.1088/1748-9326/aafc1b>, 2019.
- 485 Calafat, F. M., Chambers, D. P., and Tsimplis, M. N.: Mechanisms of decadal sea level variability in the eastern North Atlantic and the Mediterranean Sea, *Journal of Geophysical Research: Oceans*, 117, <https://doi.org/10.1029/2012JC008285>, <https://agupubs.onlinelibrary.wiley.com/doi/abs/10.1029/2012JC008285>, 2012.
- Caron, L., Ivins, E. R., Larour, E., Adhikari, S., Nilsson, J., and Blewitt, G.: GIA Model Statistics for GRACE Hydrology, *Cryosphere, and Ocean Science, Geophysical Research Letters*, 45, 2203–2212, <https://doi.org/10.1002/2017GL076644>, <https://agupubs.onlinelibrary.wiley.com/doi/abs/10.1002/2017GL076644>, 2018.
- 490 Carret, A., Johannessen, J. A., Andersen, O. B., Ablain, M., Prandi, P., Blazquez, A., and Cazenave, A.: Arctic Sea Level During the Satellite Altimetry Era, *Surveys in Geophysics*, 38, 251–275, <https://doi.org/10.1007/s10712-016-9390-2>, <https://doi.org/10.1007/s10712-016-9390-2>, 2017.
- 495 Cheng, Y., Andersen, O., and Knudsen, P.: An Improved 20-Year Arctic Ocean Altimetric Sea Level Data Record, *Marine Geodesy*, 38, 146–162, <https://doi.org/10.1080/01490419.2014.954087>, 2015.
- Church, J. and White, N.: Sea-Level Rise from the Late 19th to the Early 21st Century, *Surveys in Geophysics*, 32, 585–602, <https://doi.org/10.1007/s10712-011-9119-1>, <https://www.scopus.com/inward/record.uri?eid=2-s2.0-80053195533&doi=10.1007%2fs10712-011-9119-1&partnerID=40&md5=a6a2b9bb53f622e9bf4b3266a27d54f0>, cited By 737, 2011a.
- 500 Church, J. A. and White, N. J.: Sea-Level Rise from the Late 19th to the Early 21st Century, *Surveys in Geophysics*, 32, 585–602, <https://doi.org/10.1007/s10712-011-9119-1>, <https://doi.org/10.1007/s10712-011-9119-1>, 2011b.

- Dangendorf, S., Calafat, F. M., Arns, A., Wahl, T., Haigh, I. D., and Jensen, J.: Mean sea level variability in the North Sea: Processes and implications, *Journal of Geophysical Research: Oceans*, 119, <https://doi.org/10.1002/2014JC009901>, <https://agupubs.onlinelibrary.wiley.com/doi/abs/10.1002/2014JC009901>, 2014.
- 505 Dangendorf, S., Hay, C., Calafat, F. M., Marcos, M., Piecuch, C. G., Berk, K., and Jensen, J.: Persistent acceleration in global sea-level rise since the 1960s, *Nature Climate Change*, 9, 705–710, <https://doi.org/10.1038/s41558-019-0531-8>, 2019.
- Forget, G., Campin, J.-M., Heimbach, P., Hill, C. N., Ponte, R. M., and Wunsch, C.: ECCO version 4: an integrated framework for non-linear inverse modeling and global ocean state estimation, *Geoscientific Model Development*, 8, 3071–3104, <https://doi.org/10.5194/gmd-8-3071-2015>, <https://gmd.copernicus.org/articles/8/3071/2015/>, 2015.
- 510 Frederikse, T., Jevrejeva, S., Riva, R., and Dangendorf, S.: A consistent sea-level reconstruction and its budget on basin and global scales over 1958-2014, *Journal of Climate*, 31, 1267–1280, <https://doi.org/10.1175/JCLI-D-17-0502.1>, <https://www.scopus.com/inward/record.uri?eid=2-s2.0-85040922795&doi=10.1175%2fJCLI-D-17-0502.1&partnerID=40&md5=3a2c9a8327f26f947827ce721d43c5d4>, cited By 12, 2018.
- Frederikse, T., Landerer, F., Caron, L., Adhikari, S., Parkes, D., Humphrey, V. W., Dangendorf, S., Hogarth, P., Zanna, L., Cheng, L., and
 515 Wu, Y. H.: The causes of sea-level rise since 1900, *Nature*, 584, 393–397, <https://doi.org/10.1038/s41586-020-2591-3>, 2020.
- Fukumori, I., Wang, O., Fenty, I., Forget, G., Heimbach, P., and Ponte, R. M.: ECCO Version 4 Release 4 Dataset, accessed: 2020-06-25, 2019.
- Gill, A. and Niller, P.: The theory of the seasonal variability in the ocean, *Deep Sea Research and Oceanographic Abstracts*, 20, 141 – 177, [https://doi.org/https://doi.org/10.1016/0011-7471\(73\)90049-1](https://doi.org/https://doi.org/10.1016/0011-7471(73)90049-1), <http://www.sciencedirect.com/science/article/pii/0011747173900491>,
 520 1973.
- Gregory, J. M., Griffies, S. M., Hughes, C. W., Lowe, J. A., Church, J. A., Fukimori, I., Gomez, N., Kopp, R. E., Landerer, F., Cozannet, G. L., Ponte, R. M., Stammer, D., Tamisiea, M. E., and van de Wal, R. S. W.: Concepts and Terminology for Sea Level: Mean, Variability and Change, Both Local and Global, *Surveys in Geophysics*, 40, 1251–1289, <https://doi.org/10.1007/s10712-019-09525-z>, <https://doi.org/10.1007/s10712-019-09525-z>, 2019.
- 525 Henry, O., Prandi, P., Llovel, W., Cazenave, A., Jevrejeva, S., Stammer, D., Meyssignac, B., and Koldunov, N.: Tide gauge-based sea level variations since 1950 along the Norwegian and Russian coasts of the Arctic Ocean: Contribution of the steric and mass components, *Journal of Geophysical Research: Oceans*, 117, <https://doi.org/10.1029/2011JC007706>, <https://agupubs.onlinelibrary.wiley.com/doi/abs/10.1029/2011JC007706>, 2012.
- Holgate, S. J., Matthews, A., Woodworth, P. L., Rickards, L. J., Tamisiea, M. E., Bradshaw, E., Foden, P. R., Gordon, K. M., Jevrejeva, S.,
 530 and Pugh, J.: New Data Systems and Products at the Permanent Service for Mean Sea Level, *Journal of Coastal Research*, 29, 493–504, <https://doi.org/10.2112/JCOASTRES-D-12-00175.1>, <https://doi.org/10.2112/JCOASTRES-D-12-00175.1>, 2012.
- Khan, S. A., Sasgen, I., Bevis, M., van Dam, T., Bamber, J. L., Wahr, J., Willis, M., Kjær, K. H., Wouters, B., Helm, V., Csatho, B., Fleming, K., Bjørk, A. A., Aschwanden, A., Knudsen, P., and Munneke, P. K.: Geodetic measurements reveal similarities between post-Last Glacial Maximum and present-day mass loss from the Greenland ice sheet, *Science Advances*, 2, <https://doi.org/10.1126/sciadv.1600931>,
 535 <https://advances.sciencemag.org/content/2/9/e1600931>, 2016.
- King, M. A., Keshin, M., Whitehouse, P. L., Thomas, I. D., Milne, G., and Riva, R. E. M.: Regional biases in absolute sea-level estimates from tide gauge data due to residual unmodeled vertical land movement, *Geophysical Research Letters*, 39, <https://doi.org/10.1029/2012GL052348>, <https://agupubs.onlinelibrary.wiley.com/doi/abs/10.1029/2012GL052348>, 2012.

- Kustowski, B., Dziwion'ski, A. M., and Ekstro'm, G.: Nonlinear Crustal Corrections for Normal-Mode Seismograms, *Bulletin of the Seismological Society of America*, 97, 1756–1762, <https://doi.org/10.1785/0120070041>, <https://doi.org/10.1785/0120070041>, 2007.
- 540 Laxon, S., Peacock, H., and Smith, D.: High interannual variability of sea ice thickness in the Arctic region, *Nature*, 425, 947–950, <https://doi.org/10.1038/nature02050>, 2003.
- Limkilde Svendsen, P., Andersen, O. B., and Aasbjerg Nielsen, A.: Stable reconstruction of Arctic sea level for the 1950–2010 period, *Journal of Geophysical Research: Oceans*, 121, 5697–5710, <https://doi.org/10.1002/2016JC011685>, <https://agupubs.onlinelibrary.wiley.com/doi/abs/10.1002/2016JC011685>, 2016.
- 545 Ludwigsen, C., Khan, S. A., Andersen, O. B., and Marzeion, B.: Vertical Land Motion from present-day deglaciation in the wider Arctic, *Earth and Space Science Open Archive*, p. 18, <https://doi.org/10.1002/essoar.10502890.1>, <https://doi.org/10.1002/essoar.10502890.1>, 2020a.
- Ludwigsen, C. A. and Andersen, O. B.: Contributions to Arctic sea level from 2003 to 2015, *Advances in Space Research*, <https://doi.org/https://doi.org/10.1016/j.asr.2019.12.027>, <http://www.sciencedirect.com/science/article/pii/S0273117719309275>, 2020.
- 550 Ludwigsen, C. A., Andersen, O. B., Khan, S. A., and Marzeion, B.: Arctic Vertical Land Motion (5x5 km), <https://doi.org/10.11583/DTU.12554489.v1>, https://data.dtu.dk/articles/dataset/Arctic_Vertical_Land_Motion_5x5_km_/12554489, 2020b.
- Luthcke, S. B., Sabaka, T., Loomis, B., Arendt, A., McCarthy, J., and Camp, J.: Antarctica, Greenland and Gulf of Alaska land-ice evolution from an iterated GRACE global mascon solution, *Journal of Glaciology*, 59, 613–631, <https://doi.org/10.3189/2013JoG12J147>, 2013.
- 555 Marzeion, B., Jarosch, A. H., and Hofer, M.: Past and future sea-level change from the surface mass balance of glaciers, *The Cryosphere*, 6, 1295–1322, <https://doi.org/10.5194/tc-6-1295-2012>, <https://www.the-cryosphere.net/6/1295/2012/>, 2012.
- Melini, D., Spada, G., Gegout, P., and King, M.: REAR: a Regional ELAstic Rebound calculator. User manual for version 1.0, available on-line at: <http://hpc.rm.ingv.it/rear>., 2015.
- 560 Melkonian, A. K., Willis, M. J., Pritchard, M. E., and Stewart, A. J.: Recent changes in glacier velocities and thinning at Novaya Zemlya, *Remote Sensing of Environment*, 174, 244 – 257, <https://doi.org/https://doi.org/10.1016/j.rse.2015.11.001>, <http://www.sciencedirect.com/science/article/pii/S0034425715301899>, 2016.
- Morison, J., Kwok, R., Peralta-Ferriz, C., Alkire, M., Rigor, I., Andersen, R., and Steele, M.: Changing Arctic Ocean freshwater pathways, *Nature*, 481, 66–70, <https://doi.org/10.1038/nature10705>, <https://doi.org/10.1038/nature10705>, 2012.
- 565 Naeije, M., Schrama, E., and Scharroo, R.: The radar Altimeter Database System project RADS, 2, 487 – 490 vol.2, <https://doi.org/10.1109/IGARSS.2000.861605>, 2000.
- Peacock, N. R. and Laxon, S. W.: Sea surface height determination in the Arctic Ocean from ERS altimetry, *Journal of Geophysical Research C: Oceans*, 109, C07001 1–14, <https://doi.org/10.1029/2001JC001026>, 2004.
- Peltier, W.: Closure of the budget of global sea level rise over the GRACE era: the importance and magnitudes of the required corrections for global glacial isostatic adjustment, *Quaternary Science Reviews*, 28, 1658 – 1674, <https://doi.org/https://doi.org/10.1016/j.quascirev.2009.04.004>, <http://www.sciencedirect.com/science/article/pii/S0277379109001218>, *quaternary Ice Sheet-Ocean Interactions and Landscape Responses*, 2009.
- 570 Prandi, P., Ablain, M., Cazenave, A., and Picot, N.: A New Estimation of Mean Sea Level in the Arctic Ocean from Satellite Altimetry, *Marine Geodesy*, 35, 61–81, <https://doi.org/10.1080/01490419.2012.718222>, <https://doi.org/10.1080/01490419.2012.718222>, 2012.

- 575 Proshutinsky, A., Ashik, I. M., Dvorkin, E. N., Häkkinen, S., Krishfield, R. A., and Peltier, W. R.: Secular sea level change in the Russian sector of the Arctic Ocean, *Journal of Geophysical Research: Oceans*, 109, <https://doi.org/10.1029/2003JC002007>, <https://agupubs.onlinelibrary.wiley.com/doi/abs/10.1029/2003JC002007>, 2004.
- Pugh, D. and Woodworth, P.: *Sea-Level Science: Understanding Tides, Surges, Tsunamis and Mean Sea-Level Changes*, Cambridge University Press, <https://doi.org/10.1017/CBO9781139235778>, 2014.
- 580 Raj, R. P., Andersen, O. B., Johannessen, J. A., Gutknecht, B. D., Chatterjee, S., Rose, S. K., Bonaduce, A., Horwath, M., Rannal, H., Richter, K., Palanisamy, H., Ludwigsen, C. A., Bertino, L., Nilsen, J. E. O., Knudsen, P., Hogg, A., Cazenave, A., and Benveniste, J.: Arctic Sea level Budget Assessment During the GRACE/Argo Time Period, *Remote Sensing*, 12, <https://doi.org/10.3390/rs12172837>, <https://www.mdpi.com/2072-4292/12/17/2837>, 2020.
- Rajner, M.: Detection of ice mass variation using gnss measurements at Svalbard, *Journal of Geodynamics*, 121, 20 – 25, <https://doi.org/https://doi.org/10.1016/j.jog.2018.06.001>, <http://www.sciencedirect.com/science/article/pii/S0264370718300450>, 2018.
- 585 Ricker, R., Hendricks, S., and Beckers, J. F.: The impact of geophysical corrections on sea-ice freeboard retrieved from satellite altimetry, *Remote Sensing*, 8, 317, <https://doi.org/10.3390/rs8040317>, 2016.
- Roquet, F., Madec, G., McDougall, T. J., and Barker, P. M.: Accurate polynomial expressions for the density and specific volume of seawater using the TEOS-10 standard, *Ocean Modelling*, 90, 29 – 43, <https://doi.org/https://doi.org/10.1016/j.ocemod.2015.04.002>, <http://www.sciencedirect.com/science/article/pii/S1463500315000566>, 2015.
- 590 Rose, S. K., Andersen, O., Passaro, M., Ludwigsen, C., and Schwatke, C.: Arctic Ocean Sea Level Record from the Complete Radar Altimetry Era: 1991-2018, *Remote Sensing*, 11, <https://doi.org/10.3390/rs11141672>, 2019.
- Royston, S., Dutt Vishwakarma, B., Westaway, R., Rougier, J., Sha, Z., and Bamber, J.: Can We Resolve the Basin-Scale Sea Level Trend Budget From GRACE Ocean Mass?, *Journal of Geophysical Research: Oceans*, 125, e2019JC015535, <https://doi.org/https://doi.org/10.1029/2019JC015535>, <https://agupubs.onlinelibrary.wiley.com/doi/abs/10.1029/2019JC015535>, e2019JC015535 10.1029/2019JC015535, 2020.
- 595 Save, H., Bettadpur, S., and Tapley, B. D.: High-resolution CSR GRACE RL05 mascons, *Journal of Geophysical Research: Solid Earth*, 121, 7547–7569, <https://doi.org/10.1002/2016JB013007>, <https://agupubs.onlinelibrary.wiley.com/doi/abs/10.1002/2016JB013007>, 2016.
- Schröder, L., Horwath, M., Dietrich, R., Helm, V., van den Broeke, M. R., and Ligtenberg, S. R. M.: Four decades of Antarctic surface elevation changes from multi-mission satellite altimetry, *The Cryosphere*, 13, 427–449, <https://doi.org/10.5194/tc-13-427-2019>, <https://www.the-cryosphere.net/13/427/2019/>, 2019.
- 600 Shepherd, A., Ivins, E., Rignot, E., Smith, B., van den Broeke, M., Velicogna, I., Whitehouse, P. L., Briggs, K., Joughin, I., Krinner, G., Nowicki, S., Payne, T., Scambos, T., Schlegel, N., A. G., Agosta, C., Ahlstrøm, A., Babonis, G., Barletta, V., Blazquez, A., Bonin, J., Csatho, B., Cullather, R., Felikson, D., Fettweis, X., Forsberg, R., Gallee, H., Gardner, A., Gilbert, L., Groh, A., Gunter, B., Hanna, E., Harig, C., Helm, V., Horvath, A., Horwath, M., Khan, S., K. Kjeldsen, K., Konrad, H., Langen, P., Lecavalier, B., Loomis, B., Luthcke, S., McMillan, M., Melini, D., Mernild, S., Mohajerani, Y., Moore, P., Mouginit, J., Moyano, G., Muir, A., Nagler, T., Nield, G., Nilsson, J., Noel, B., Ootaka, I., E. Pattle, M., Peltier, W. R., Pie, N., Rietbroek, R., Rott, H., Sandberg-Sørensen, L., Sasgen, I., Save, H., Scheuchl, B., Schrama, E., Schröder, L., Seo, K.-W., Simonsen, S., Slater, T., Spada, G., Sutterley, T., Talpe, M., Tarasov, L., van de Berg, W. J., van der Wal, W., van Wessem, M., Dutt Vishwakarma, B., Wiese, D., and Wouters, B.: Mass balance of the Antarctic Ice Sheet from 1992 to 2017, *Nature*, 558, 219–222, <https://doi.org/10.1038/s41586-018-0179-y>, 2018.
- 610 Shepherd, A., Ivins, E., Rignot, E., Smith, B., van den Broeke, M., Velicogna, I., Whitehouse, P., Briggs, K., Joughin, I., Krinner, G., Nowicki, S., Payne, T., Scambos, T., Schlegel, N., Geruo, A., Agosta, C., Ahlstrøm, A., Babonis, G., Barletta, V. R., Bjørk, A. A., Blazquez, A.,

- Bonin, J., Colgan, W., Csatho, B., Cullather, R., Engdahl, M. E., Felikson, D., Fettweis, X., Forsberg, R., Hogg, A. E., Gallee, H., Gardner, A., Gilbert, L., Gourmelen, N., Groh, A., Gunter, B., Hanna, E., Harig, C., Helm, V., Horvath, A., Horwath, M., Khan, S., Kjeldsen, K. K., Konrad, H., Langen, P. L., Lecavalier, B., Loomis, B., Luthcke, S., McMillan, M., Melini, D., Mernild, S., Mohajerani, Y., Moore, P., Mottram, R., Mouginit, J., Moyano, G., Muir, A., Nagler, T., Nield, G., Nilsson, J., Noël, B., Otosaka, I., Pattle, M. E., Peltier, W. R., Pie, N., Rietbroek, R., Rott, H., Sørensen, L. S., Sasgen, I., Save, H., Scheuchl, B., Schrama, E., Schröder, L., Seo, K.-W., Simonsen, S. B., Slater, T., Spada, G., Sutterley, T., Talpe, M., Tarasov, L., Jan van de Berg, W., van der Wal, W., van Wessem, M., Vishwakarma, B. D., Wiese, D., Wilton, D., Wagner, T., Wouters, B., Wuite, J., and Team, T. I.: Mass balance of the Greenland Ice Sheet from 1992 to 2018, *Nature*, 579, 233–239, <https://doi.org/10.1038/s41586-019-1855-2>, 2020.
- Smith, G. C., Allard, R., Babin, M., Bertino, L., Chevallier, M., Corlett, G., Crout, J., Davidson, F., Delille, B., Gille, S. T., Hebert, D., Hyder, P., Intrieri, J., Lagunas, J., Larnicol, G., Kaminski, T., Kater, B., Kauker, F., Marec, C., Mazloff, M., Metzger, E. J., Mordy, C., O’Carroll, A., Olsen, S. M., Phelps, M., Posey, P., Prandi, P., Rehm, E., Reid, P., Rigor, I., Sandven, S., Shupe, M., Swart, S., Smedstad, O. M., Solomon, A., Storto, A., Thibaut, P., Toole, J., Wood, K., Xie, J., Yang, Q., and , t. W. P. S. G.: Polar Ocean Observations: A Critical Gap in the Observing System and Its Effect on Environmental Predictions From Hours to a Season, *Frontiers in Marine Science*, 6, 429, <https://doi.org/10.3389/fmars.2019.00429>, <https://www.frontiersin.org/article/10.3389/fmars.2019.00429>, 2019.
- Spada, G.: Glacial Isostatic Adjustment and Contemporary Sea Level Rise: An Overview, *Surveys in Geophysics*, 38, 153–185, <https://doi.org/10.1007/s10712-016-9379-x>, <https://doi.org/10.1007/s10712-016-9379-x>, 2017.
- Stammer, D.: Steric and wind-induced changes in TOPEX/POSEIDON large-scale sea surface topography observations, *Journal of Geophysical Research: Oceans*, 102, 20 987–21 009, <https://doi.org/10.1029/97JC01475>, <https://agupubs.onlinelibrary.wiley.com/doi/abs/10.1029/97JC01475>, 1997.
- Stammer, D., Ray, R. D., Andersen, O. B., Arbic, B. K., Bosch, W., Carrère, L., Cheng, Y., Chinn, D. S., Dushaw, B. D., Egbert, G. D., Erofeeva, S. Y., Fok, H. S., Green, J. A. M., Griffiths, S., King, M. A., Lapin, V., Lemoine, F. G., Luthcke, S. B., Lyard, F., Morison, J., Müller, M., Padman, L., Richman, J. G., Shriver, J. F., Shum, C. K., Taguchi, E., and Yi, Y.: Accuracy assessment of global barotropic ocean tide models, *Reviews of Geophysics*, 52, 243–282, <https://doi.org/10.1002/2014rg000450>, 2014.
- van Dam, T., Collilieux, X., Wuite, J., Altamimi, Z., and Ray, J.: Nontidal ocean loading: amplitudes and potential effects in GPS height time series, *Journal of Geodesy*, 86, 1043–1057, <https://doi.org/10.1007/s00190-012-0564-5>, <https://doi.org/10.1007/s00190-012-0564-5>, 2012.
- Wang, H., Xiang, L., Jia, L., Jiang, L., Wang, Z., Hu, B., and Gao, P.: Load Love numbers and Green’s functions for elastic Earth models PREM, iasp91, ak135, and modified models with refined crustal structure from Crust 2.0, *Computers & Geosciences*, 49, 190 – 199, <https://doi.org/https://doi.org/10.1016/j.cageo.2012.06.022>, <http://www.sciencedirect.com/science/article/pii/S0098300412002245>, 2012.
- WCRP, G. S. L. B. G.: Global sea-level budget 1993–present, *Earth System Science Data*, 10, 1551–1590, <https://doi.org/10.5194/essd-10-1551-2018>, <https://essd.copernicus.org/articles/10/1551/2018/>, 2018.
- Wiese, D. N., Landerer, F. W., and Watkins, M. M.: Quantifying and reducing leakage errors in the JPL RL05M GRACE mascon solution, *Water Resources Research*, 52, 7490–7502, <https://doi.org/10.1002/2016WR019344>, <https://agupubs.onlinelibrary.wiley.com/doi/abs/10.1002/2016WR019344>, 2016.
- Zemp, M., Huss, M., Thibert, E., Eckert, N., McNabb, R., Huber, J., Barandun, M., Machguth, H., Nussbaumer, S. U., Gärtner-Roer, I., Thomson, L., Paul, F., Maussion, F., Kutuzov, S., and Cogley, J. G.: Global glacier mass changes and their contributions to sea-level rise from 1961 to 2016, *Nature*, 568, 382–386, <https://doi.org/10.1038/s41586-019-1071-0>, 2019.